The dielectric constant of polar fluids and the distribution of the total dipole moment

P. G. Kusalik, M. E. Mandy,[a] and I. M. Svishchev
Department of Chemistry, Dalhousie University, Halifax, Nova Scotia B3H 4J3, Canada

(Received 1 October 1993; accepted 2 February 1994)

This article examines the distribution of fluctuations of the total dipole moment **M** in polar fluids. Detailed results, including average energies, pressures, and dielectric constants, are reported from molecular dynamics simulations of a dipolar soft-sphere system in reaction field (RF) and periodic boundary conditions (PBC). Both cubic and truncated octahedral simulation cells are employed and we demonstrate that the properties of interest are insensitive to our choice of cell geometry. Some dependence upon RF cutoff is observed, particularly in results for the static dielectric constant. The distribution of instantaneous values of **M** shows no anisotropy, and we argue that the isotropic probability distribution function $P(g)$, where g is the Kirkwood correlation factor and depends only upon the magnitude of **M**, is sufficient to fully characterize the fluctuations in the total moment for a large sample of a polar liquid. We demonstrate that the functional form for $P(g)$ previously tested for a dipolar fluid in PBC [P. G. Kusalik, Mol. Phys. **80**, 225 (1993)] holds for RF boundary conditions; we also find that this form is obeyed by other polar liquids such as water and methanol. The distribution function $P(g)$ is found to be particularly effective at detecting finite size effects in simulations of polar liquids. We also show how knowledge of the functional form for $P(g)$ can be efficaciously used to achieve significant reductions in the computational resources required to determine a static dielectric constant for a polar liquid.

I. INTRODUCTION

The static dielectric constant ϵ is a fundamental property of polar liquids[1] and thus remains a major focus of research interest. Presently, much of our insight into this area comes from computer simulation. Unfortunately, the determination of ϵ by computer simulation has presented both conceptual[2–7] and computational difficulties.[7–16] While many of the formal problems have now been resolved, important questions concerning methodology and its implementation remain. Furthermore, lengthy simulations are usually required to determine reasonably precise (although not necessarily accurate) values for the static dielectric constant for highly polar liquids, such as water. Clearly, more efficient computational routes to ϵ are desirable, along with a fuller understanding of the influences of sample size and boundary conditions upon the dielectric properties of polar liquids.

Conventionally, in a computer simulation ϵ has been obtained from the fluctuations in the total dipole moment of the system **M** through the standard relationship[3–5]

$$\frac{(\epsilon-1)(2\epsilon_{RF}+1)}{2\epsilon_{RF}+\epsilon}=\frac{4\pi}{3V}\frac{\langle M^2\rangle}{kT}=3y\langle g\rangle, \tag{1}$$

in which ϵ_{RF} is the dielectric constant of the continuum surrounding the system (e.g., $\epsilon_{RF}=1$ for an isolated system), V is the volume, $y=4\pi\rho\mu^2/9kT$, and

$$g=\frac{M^2}{N\mu^2}. \tag{2}$$

In the above expressions $\rho=N/V$ is the number density, N is the number of particles in the system, and μ is the molecular dipole moment. Here, the Kirkwood correlation factor g, as defined by Eq. (2), is an instantaneous rather than an average quantity. Equation (1) has been shown[3,5] to be valid for both reaction field (RF) and periodic boundary conditions (PBC), although deLeeuw *et al.*[2] have argued that in RF boundary conditions a more appropriate expression for ϵ is

$$\frac{(\epsilon-1)(2\epsilon_{RF}+1)}{(2\epsilon_{RF}+\epsilon)}=\frac{1}{R_c^3kT}\langle\mathbf{M}\cdot\mathbf{M}(R_c)\rangle, \tag{3}$$

in which $\mathbf{M}(R_c)$ is just the total moment of a spherical sample of volume $\Omega=4\pi R_c^3/3$, where R_c is the reaction field cut-off distance. As we will be making direct comparisons between simulation results for ϵ from both periodic and RF boundary conditions, it is important to clarify the relationship between Eqs. (1) and (3). In the Appendix we have shown that for a dense fluid and large Ω Eqs. (1) and (3) become equivalent. In the present study we will use $\langle M^2\rangle$ exclusively as our measure of the susceptibility of our polar fluids in either boundary condition; hence all dielectric constants reported are those obtained with Eq. (1). At the same time we will analyze the extent to which the equivalence of Eqs. (1) and (3) holds for systems of a few hundred particles.

Other approaches by which to obtain ϵ from a computer simulation have been attempted by many workers, including applied field calculations[9,11,16] where one simply measures the average polarization, transient response methods[17,18] in which the time-dependent (nonequilibrium) polarization response is monitored, constant polarization calculations[19] where one observes the average field required to maintain a fixed polarization, and calculations with rather large systems[15] which allow one to extract ϵ from the long-range dependence of the dipole–dipole correlations. Although all these approaches have been employed successfully to extract

[a]Present address: Department of Physics, University of Toronto, Toronto, Ontario M5S 1A7, Canada.

 0021-9606/94/100(10)/7854/11/$6.00

a value for the static dielectric constant, none has proven to be markedly superior computationally to Eq. (1), considering the total time used by the calculation and the statistical uncertainties obtained. Our interest in trying to develop more efficient routes to ϵ and in improving our understanding of the effects of finite sample size and boundary conditions has refocused our attention onto the fluctuations in the total dipole moment.

In this article we consider the distribution of values of $\mathbf{M}$ and show that it can be characterized by the isotropic probability distribution function $P(g)$. In an earlier communication[20] we have formally demonstrated that $P(g)$ possesses a relatively simple functional form. The behavior of this distribution function is examined in detail, in particular its dependence upon system size and boundary conditions. Our previous simulation work with dipolar fluids[14] has strongly suggested that the rather slow convergence of $\langle M^2 \rangle$ is partially due to poor sampling of large but rare fluctuations in the total moment. In this work we demonstrate how a functional form for $P(g)$ can be exploited to help circumvent such difficulties thereby leading to computationally efficient routes to the dielectric constant.

In the very recent and independent work of Chandler and co-workers,[13] they have employed umbrella sampling molecular dynamics to construct the total moment probability distribution function $P(\mathbf{M})$ for a water-like liquid by fitting together results from many individual molecular dynamics calculations which each sampled a particular window in $\mathbf{M}$. Chandler has reported a significant improvement in the convergence of $\langle M^2 \rangle$ using this technique. In the present study we have also carried out molecular dynamics simulations in which only specific windows in g have been sampled. We demonstrate that with a functional form for $P(g)$, $\langle g \rangle$ (and hence ϵ) may be determined reliably while sampling only a limited range of the values in g.

II. SIMULATION DETAILS

The present dipolar soft-sphere model and details of our general molecular dynamics simulation methodology have been described previously,[14] and therefore here we only briefly outline some key points.

In the current investigation we have focused upon a dipolar soft-sphere fluid for which the energy of interaction $u(12)$ between any two particles 1 and 2 is simply the sum of the soft-sphere potential,

$$u_{ss}(r) = 4\epsilon_{ss}\left(\frac{\sigma}{r}\right)^{12}, \tag{4a}$$

and the dipole–dipole interaction,

$$u_{dd}(12) = -3(\boldsymbol{\mu}_1 \cdot \mathbf{r})(\boldsymbol{\mu}_2 \cdot \mathbf{r})/r^5 + \boldsymbol{\mu}_1 \cdot \boldsymbol{\mu}_2 / r^3, \tag{4b}$$

where $\boldsymbol{\mu}_i$ is the dipole moment on particle i and $\mathbf{r} = \mathbf{r}_2 - \mathbf{r}_1$ is the separation vector. This dipolar system had been studied in both periodic and RF boundary conditions, and both cubic and truncated octahedral geometries for the basic simulation cell have been exploited.

In periodic boundary conditions, the required lattice sums have been evaluated with the Ewald summation technique.[2,21] The extension of the standard Ewald summation expressions[21] for cubic geometry to truncated octahedral cells involves only the trivial additions of the appropriate factors of 2 and the selection of reciprocal space vectors consistent with an fcc lattice.[22] As in previous work,[14,15] care was taken in choosing the truncation points and the value of the unitless convergence parameter α so as to ensure a negligible influence upon the properties of interest. For our simulations in PBC, the real space sum was carried over all nearest images (with the exception of our 864 particle systems where a spherical cutoff was employed[14,15]), while in reciprocal space only those vectors $\mathbf{n}$ for which $n^2 \leq n^2_{max}$ were included. Values for n^2_{max} and α used in the present calculations are given in Table I. For cubic samples n^2_{max} and α are the same as in our earlier work,[14] while for truncated octahedral cells these values were selected to retain comparable levels of accuracy in the determination of the total energy. Whereas it may appear from Table I that simulation runs for truncated octahedral samples would be slower in executing, they are in practice slightly faster since the number of unique vectors considered in the Fourier space sum was always less (by typically 10%–15%) than for cubic geometry.

TABLE I. Values of the Ewald parameters n^2_{max} and α employed in the present study for cubic and truncated octahedral geometry.

	Cubic		Truncated octahedral	
N	n^2_{max}	α	n^2_{max}	α
32	54	5.75	73	7.0
108	42	5.75	65	7.0
256	38	5.75	55	6.75
500	30	5.75	49	6.75
864[a]	70	7.75	...	...

[a]Spherical truncation at $R_c = 0.41$ in real space sum.

TABLE II. Results for cubic samples of a dipolar soft-sphere fluid in periodic boundary conditions at $\rho^* = 0.8$, $T^* = 1.35$, and $\mu^* = 2.0$. The values for ϵ given in parentheses are estimates of the uncertainties.

ϵ_{RF}	$\langle U_{DD} \rangle / N\epsilon_{ss}$[a]	$\langle U \rangle / N\epsilon_{ss}$[a]	$p\sigma^3/\epsilon_{ss}$	$\langle g \rangle$	ϵ
		32 particles			
100	−6.056	−0.649	13.50	5.964	85.0 (±2.0)
∞	−6.107	−0.710	13.45	7.311	73.6 (±1.0)
		108 particles			
1	−5.990	−0.617	13.46	0.296	135 (±25)
100	−6.036	−0.673	13.40	6.279	91.4 (±2.5)
∞[b]	−6.060	−0.698	13.39	8.741	87.8 (±2.0)
∞[b]	−6.056	−0.695	13.38	8.462	85.0 (±2.0)
		256 particles			
100	−6.053	−0.664	13.48	6.755	101.7 (±3.0)
∞	−6.061	−0.679	13.45	9.758	97.9 (±3.0)
		500 particles			
100	−6.055	−0.668	13.47	6.554	97.2 (±4.0)
∞	−6.061	−0.675	13.47	9.884	99.1 (±3.0)
		864 particles			
100	−6.055	−0.669	13.47	6.549	97.1 (±2.0)
∞	−6.056	−0.672	13.46	9.868	99.0 (±3.0)

[a]Includes boundary term as discussed in the text.
[b]Two independent runs for $N = 108$ and $\epsilon_{RF} = \infty$.

TABLE III. Results for truncated octahedral samples of a dipolar soft-sphere fluid in periodic boundary conditions at $\rho^*=0.8$, $T^*=1.35$, and $\mu^*=2.0$. The values for ϵ given in parentheses are estimates of the uncertainties.

ϵ_{RF}	$\langle U_{DD}\rangle/N\epsilon_{ss}$[a]	$\langle U\rangle/N\epsilon_{ss}$[a]	$p\sigma^3/\epsilon_{ss}$	$\langle g\rangle$	ϵ
		32 particles			
10	−5.960	−0.481	13.79	1.872	163 (±20.)
100	−6.095	−0.637	13.64	5.781	81.3 (±2.0)
∞	−6.155	−0.691	13.63	7.045	71.0 (±2.0)
		108 particles			
10	−6.022	−0.604	13.58	1.789	117 (±8.0)
100	−6.062	−0.650	13.54	6.370	93.3 (±1.5)
∞	−6.081	−0.673	13.52	8.720	87.6 (±2.0)
		256 particles			
10	−6.037	−0.645	13.50	1.763	106.2 (±6.0)
100	−6.053	−0.662	13.48	6.469	95.4 (±3.5)
∞	−6.065	−0.674	13.48	9.728	97.6 (±2.0)
		500 particles			
10	−6.047	−0.660	13.48	1.770	108.8 (±8.0)
100	−6.052	−0.666	13.47	6.577	97.7 (±3.0)
∞	−6.059	−0.673	13.47	9.660	96.9 (±2.5)

[a]Includes boundary term as discussed in the text.

Our simulations in RF boundary conditions were performed using standard techniques.[21] With only a single exception, the reaction field cut-off distance R_c was always set to its maximum value equal to the radius of the inscribed sphere. No attempt was made to taper the potential function at its discontinuity at R_c.

Molecular dynamics (MD) simulations were carried out at constant temperature for systems of 32, 108, 256, 500, and 864 dipolar soft spheres, isothermal conditions being maintained with the aid of a Gaussian thermostat.[23] This dipolar fluid can be characterized by a reduced density,

$$\rho^*=\rho\sigma^3=0.8, \tag{5a}$$

a reduced temperature,

$$T^*=kT/\epsilon_{ss}=1.35, \tag{5b}$$

and a reduced dipole moment,

$$\mu^*=(\mu^2/\epsilon_{ss}\sigma^3)^{1/2}=2.0. \tag{5c}$$

This fluid has already been extensively studied in PBC,[14–16] from which an accurate estimate of 98 ± 2 for the infinite system dielectric constant can be obtained. In the current investigation four different values for ϵ_{RF} (1, 10, 100, and ∞) have been employed. Tables II and III detail the runs we have performed in PBC for cubic and truncated octahedral geometries, respectively. The results reported in Tables II and III were obtained from trajectories of at least 500 000 time steps (1250 reduced time units). Tables IV and V, respectively, summarize the MD simulations carried out in RF boundary conditions for cubic and truncated octahedral geometries where our runs were a minimum of 400 000 time steps (1000 reduced time units) in length. Equilibration periods were typically 20 000–25 000 time steps (50.0–62.5 reduced time units).

We have also carried out several MD simulations in which only specific windows (or ranges of values for g) of the probability distribution function $P(g)$ were sampled. Chandler and co-workers[13] achieved this in their MD calculations by imposing an additional ramped potential function at the boundaries of the desired window. We have imposed the requirement that g remain within a specified range of values in our MD simulations by utilizing trajectory (or phase space) mapping.[18,23,24] Our implementation of this technique works as follows. When the current trajectory reaches a window boundary (as measured by g) a time reversal mapping is applied to the orientational coordinates only, taking $\dot{\mathbf{M}}\Rightarrow-\dot{\mathbf{M}}$ or $\dot{g}\Rightarrow-\dot{g}$, thus generating a new phase point of equal probability which serves as the starting point of a new trajectory. This new trajectory is then followed until a window boundary is again encountered. Hence the final distribution function obtained is an average over many shorter trajectories (rather than a single long trajectory) which are all confined to a specific window in g. The approach of Chandler and co-workers[13] should become equivalent to our technique in the limit of an infinitely steep potential function.

Two additional points are noteworthy. There is a possi-

TABLE IV. Results for cubic samples of a dipolar soft-sphere fluid in reaction field boundary conditions at $\rho^*=0.8$, $T^*=1.35$, and $\mu^*=2.0$. The values for ϵ given in parentheses are estimates of the uncertainties.

ϵ_{RF}	R_c	$\langle U_{DD}\rangle/N\epsilon_{ss}$[a]	$\langle U\rangle/N\epsilon_{ss}$[a]	$\langle g\rangle$	$\frac{\langle \mathbf{M}\cdot\mathbf{M}(R_c)\rangle}{\langle M^2\rangle}\frac{V}{\Omega}$[b]	ϵ[c]
			108 particles			
100	2.565σ	−6.047	−0.700	5.923	1.0094	84.1 (±2.5)
			256 particles			
10	3.420σ	−6.038	−0.650	1.812	1.0061	126 (±12)
100	3.420σ	−6.055	−0.686	7.083	1.0063	109.2 (±6.0)
∞	3.420σ	−6.075	−0.705	10.188	1.0061	102.2 (±2.5)
			500 particles			
100[d]	4.275σ	−6.056	−0.674	7.014	1.0023	107.6 (±4.0)
			864 particles			
100	5.130σ	−6.055	−0.671	6.661	1.0006	99.6 (±3.5)

[a]Include boundary term as discussed in the text.
[b]This ratio will be 1 when Eqs. (1) and (3) are equivalent (see the Appendix).
[c]Determined with Eq. (1).
[d]600 000 time step run.

TABLE V. Results for truncated octahedral samples of a dipolar soft-sphere fluid in reaction field boundary conditions at $\rho^*=0.8$, $T^*=1.35$, and $\mu^*=2.0$. The values for ϵ given in parentheses are estimates of the uncertainties.

ϵ_{RF}	R_c	$\langle U_{DD}\rangle/N\epsilon_{ss}$ [a]	$\langle U\rangle/N\epsilon_{ss}$ [a]	$\langle g\rangle$	$\frac{\langle \mathbf{M}\cdot\mathbf{M}(R_c)\rangle}{\langle M^2\rangle}\frac{V}{\Omega}$ [b]	ϵ [c]
			108 particles			
1	2.799σ	−6.048	−0.633	0.294	0.9861	111.6(±30.)
10	2.799σ	−5.939	−0.533	1.666	0.9871	78.9(±4.0)
100	2.799σ	−5.979	−0.579	5.063	0.9871	68.0(±2.0)
∞	2.799σ	−5.993	−0.598	6.300	0.9872	63.6(±2.0)
			256 particles			
1	3.732σ	−6.130	−0.745	0.289	0.9959	67.1(±8.0)
10	3.732σ	−6.007	−0.618	1.707	0.9968	88.8(±2.5)
100[d]	3.732σ	−6.031	−0.645	5.997	0.9969	85.6(±2.0)
100	3.434σ[e]	−6.066	−0.679	6.905	1.0054	105.1(±4.0)
∞	3.732σ	−6.043	−0.659	8.204	0.9968	82.5(±2.5)
			500 particles			
100	4.664σ	−6.045	−0.662	6.177	0.9992	89.3(±3.0)

[a]Include boundary term as discussed in the text.
[b]This ratio will be 1 when Eqs. (1) and (3) are equivalent (see the Appendix).
[c]Determined with Eq. (1).
[d]600 000 time step run.
[e]Value of R_c less than the radius of the inscribed sphere.

bility with this technique that a trajectory might be encountered which becomes trapped against a wall as a result of approaching the window boundary tangentially. In our implementation we monitored for occurrences of trajectories becoming trapped in this manner, but observed none (i.e., all trajectories were at least ten time steps in length). We did find that care was required in selecting a width for the window. Obviously, too wide a window would reduce efficiency; yet we found that with too narrow a range in g (i.e., $g_{upper}-g_{lower}\leq 5$) the system was able to traverse the window in relatively few time steps and tended to become trapped in a localized part of the orientational phase space (i.e., each successive trajectory would virtually retrace the path of the preceding one as measured by the value of g). Chandler and co-workers[13] observed an analogous effect (strong oscillations in the total moment autocorrelation function) with small windows. In our work we found that a width $g_{upper}-g_{lower}=7.5$ represented a reasonable compromise, giving an average trajectory length of typically several hundred time steps.

In order to provide additional results from other polar liquids, we have accumulated data for $P(g)$ in MD simulations of simple point charge models[25,26] for both water and methanol at 25 °C. The 108 and 256 particle runs performed with SPC/E water[25] were both 0.5 ns in length and gave values[27] of 68.8 ± 7.4 and 71.0 ± 6.1, respectively, for ϵ. Our single 108 particle methanol simulation, representing a 1.0 ns trajectory, yielded[28] a static dielectric constant of 31.5 ± 4.0. Details of our simulation methodology are reported in Refs. 27 and 28.

III. RESULTS AND DISCUSSION

In Tables II–V we report values for the average dipole–dipole energy $\langle U_{DD}\rangle/N\epsilon_{ss}$, the average total configurational energy $\langle U\rangle/N\epsilon_{ss}$, the pressure $p\sigma^3/\epsilon_{ss}$, the average value of g, and the static dielectric constant. Unlike our previously published results in PBC,[14] the average per particle energies given in Tables II and III contain the appropriate boundary condition dependent term,[21]

$$\frac{U(\epsilon_{RF})}{N}-\frac{U(\infty)}{N}=\frac{\Delta U(\epsilon_{RF},\infty)}{N}=\frac{2\pi\rho\mu^2}{N(2\epsilon_{RF}+1)}\langle g\rangle. \tag{6}$$

Inclusion of this term allows energies from simulations employing PBC to be compared directly with RF data (given in Tables IV and V) for the corresponding values of ϵ_{RF}. Numerical values of $\Delta U(\epsilon_{RF},\infty)/N\epsilon_{ss}$ are typically very small [e.g., for $N=108$ and $\epsilon_{RF}=100$, $\Delta U(100,\infty)/N\epsilon_{ss}$ represents only a 0.1% correction to the dipole–dipole energy] and decrease with increasing N. Statistical uncertainties in the average energies, pressures, and dielectric constants were obtained from an analysis of block averages. Our error estimates for the average energies and pressure are very similar to those from our earlier investigation of this system;[14] uncertainties in ϵ have been explicitly included in Tables II–V.

The current results for the thermodynamic properties and the dielectric constant of this dipolar soft-sphere fluid in PBC (Tables II and III) are in very good agreement with our previous work.[14] For smaller systems, $N=32$ and 108, we observe some sensitivity to the sample geometry, particularly in the thermodynamic properties. Yet, the dependence exhibited in Tables II and III is rather weak and for moderate size systems (i.e., 256 particles) the values appear invariant to the choice of either a cubic or truncated octahedral simulation cell. In our results for RF boundary conditions (Tables IV and V) there *appears* to be a much stronger dependence upon sample geometry, particularly in the values for ϵ.

To explore more fully the influence of geometry, sample size, and boundary condition applied upon the value of the dielectric constant obtained from a computer simulation, we

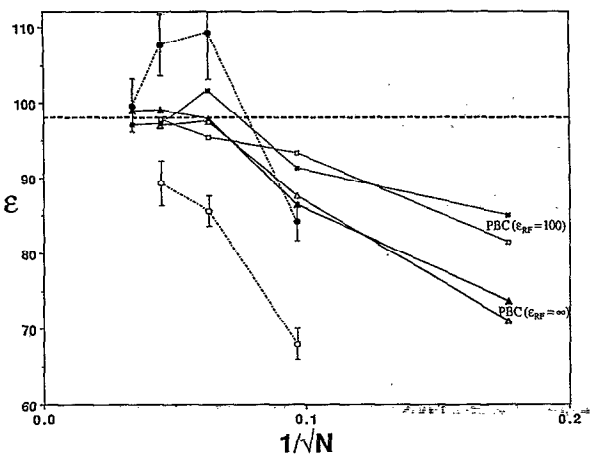

FIG. 1. System size dependence of ϵ for a dipolar soft-sphere fluid at $\rho^*=0.8$, $T^*=1.35$, and $\mu^*=2.0$. The open and solid squares are, respectively, values from truncated octahedral and cubic samples in PBC at $\epsilon_{RF}=100$, while the open and solid triangles are the respective results at $\epsilon_{RF}=\infty$. The open circles and dots represent values obtained for RF boundary conditions at $\epsilon_{RF}=100$ for truncated octahedral and cubic simulations, respectively. The heavy dashed line represents our best estimate for the infinite system dielectric constant (Refs. 14–16).

have plotted in Fig. 1 results for ϵ as a function of $1/\sqrt{N}$ for sets of runs in RF and PBC for both cubic and truncated octahedral geometries. One would expect the leading order saturation effects in ϵ to scale as $1/\sqrt{N}$, as Chandler[13] has noted, and therefore we have chosen $1/\sqrt{N}$ as the independent variable in Fig. 1.

Several important observations can be made from Fig. 1. First, all the sets of data can be extrapolated to our estimate[14–16] of 98 ± 2 for the infinite system dielectric constant. It is clear that the dependence on system size is much stronger in RF boundary conditions, while with PBC the $\epsilon_{RF}\approx\epsilon$ results demonstrate the most rapid convergence. We find again that *in PBC* ϵ is essentially independent of sample shape, and henceforth in our analysis and discussion of data obtained in PBC we will make no further distinction based on the geometry of the simulation cell. However, in Fig. 1 the geometry of the system *appears* to be a much more important consideration in RF boundary conditions. Returning to Tables IV and V, we recall that our RF calculations for cubic and truncated octahedral geometries also differed in the values employed for R_c. To establish the importance of the cut-off radius, we have performed a single additional 256 particle calculation in truncated octahedral geometry for which R_c was essentially equal to the cutoff used for the comparable cubic system (and hence smaller than the radius of the inscribed sphere). Rather strikingly, the value of ϵ obtained from this 256 particle simulation is statistically indistinguishable from the cubic result. This strongly suggests that the behavior exhibited by our RF data in Fig. 1 is not a sample geometry dependence, but is in fact a sensitivity to cut-off distance. Exploratory studies carried out with smaller cutoffs and larger systems all support this claim and indicate that the effect becomes smaller with increasing sample size.

In the Appendix we have made the assumption that the fluctuations in the number of particles in the volume Ω are small and show that Eqs. (1) and (3) are equivalent when $\langle \mathbf{M}\cdot\mathbf{M}(R_c)\rangle/\langle M^2\rangle$ equals the ratio Ω/V. Inspection of the values for $\langle \mathbf{M}\cdot\mathbf{M}(R_c)\rangle/\langle M^2\rangle V/\Omega$ in Tables IV and V reveals that even for the smallest system studied ($N=108$) this is already true to within about 1%. Interestingly, when $\langle \mathbf{M}\cdot\mathbf{M}(R_c)\rangle/\langle M^2\rangle V/\Omega$ is less than one, our simulation results tend to underestimate ϵ, whereas when it is greater than one the opposite is usually true. Clearly then, for $\epsilon_{RF}\geqslant\epsilon$ the difference between the results predicted by Eqs. (1) and (3) will be negligible, and henceforth we will focus exclusively upon the fluctuations in the *total* moment of the system. We remark that data for $\langle M(R_c)^2\rangle$ was also accumulated in our RF calculations and in all cases was found to be significantly smaller than $\langle \mathbf{M}\cdot\mathbf{M}(R_c)\rangle$ (even for $N=864$ the difference exceeded 25%).

As a first step in the characterization of the fluctuations of the total dipole moment, we consider the probability distribution function $P(\mathbf{M})$, which in general may depend on both the direction and magnitude of $\mathbf{M}$. In an isotropic liquid $P(\mathbf{M})$ obviously must be invariant to the choice of direction. In PBC, the system may be visualized as a macroscopic *spherical* sample composed of a large number of replicas of the basic cell. Yet the nonspherical simulation cells making up the macroscopic sample do not pack isotropically (cubic cells pack in a cubic structure, truncated octahedron pack in a body-centered cubic structure) and hence could perhaps give rise to anisotropy in the system. In RF boundary conditions spherical symmetry is more directly imposed through the spherical cutoff. To test for possible anisotropy in the total moment for our dipolar fluids we have measured the probabilities of finding $\mathbf{M}$ within 15 deg of any of three specific orientations, pointing into a face of the cube (100), pointing at an edge of the cube (110), or directed into a corner of the cube (111). In Table VI we have given these probabilities relative to their ideal values (which assume spherical symmetry) for various cubic systems of 108 and 864 particles in PBC. To explore the possibility of anisotropy in the magnitude of $\mathbf{M}$, values for $\langle M^2\rangle$ have also been in-

TABLE VI. Anisotropy of the total moment for cubic samples of dipolar soft spheres in PBC at $\rho^*=0.8$, $T^*=1.35$, and $\mu^*=2.0$. The relative probabilities differences attempt to measure a preferred direction, while the ratios of the fluctuations in those directions to the global (spherical) average should detect anisotropy in the magnitude of M.

	$\frac{P_{(xxx)}-P^0_{(xxx)}}{P^0_{(xxx)}}$			$\frac{\langle M^2\rangle_{(xxx)}}{\langle M^2\rangle}$		
Run	(100)	(110)	(111)	(100)	(110)	(111)
$N=108$, $\epsilon_{RF}=1$	−0.01	0.00	−0.01	1.00	1.01	0.99
$N=108$, $\epsilon_{RF}=100$	0.02	0.01	−0.03	1.01	1.02	0.95
$N=108$, $\epsilon_{RF}=\infty$	0.09	−0.05	0.01	1.05	0.98	1.00
$N=108$, $\epsilon_{RF}=\infty$	0.01	0.00	0.00	1.00	1.01	0.99
$N=864$, $\epsilon_{RF}=100$	0.06	−0.01	−0.06	1.03	0.99	0.97
$N=864$, $\epsilon_{RF}=\infty$	−0.02	−0.04	0.08	0.93	0.97	1.07

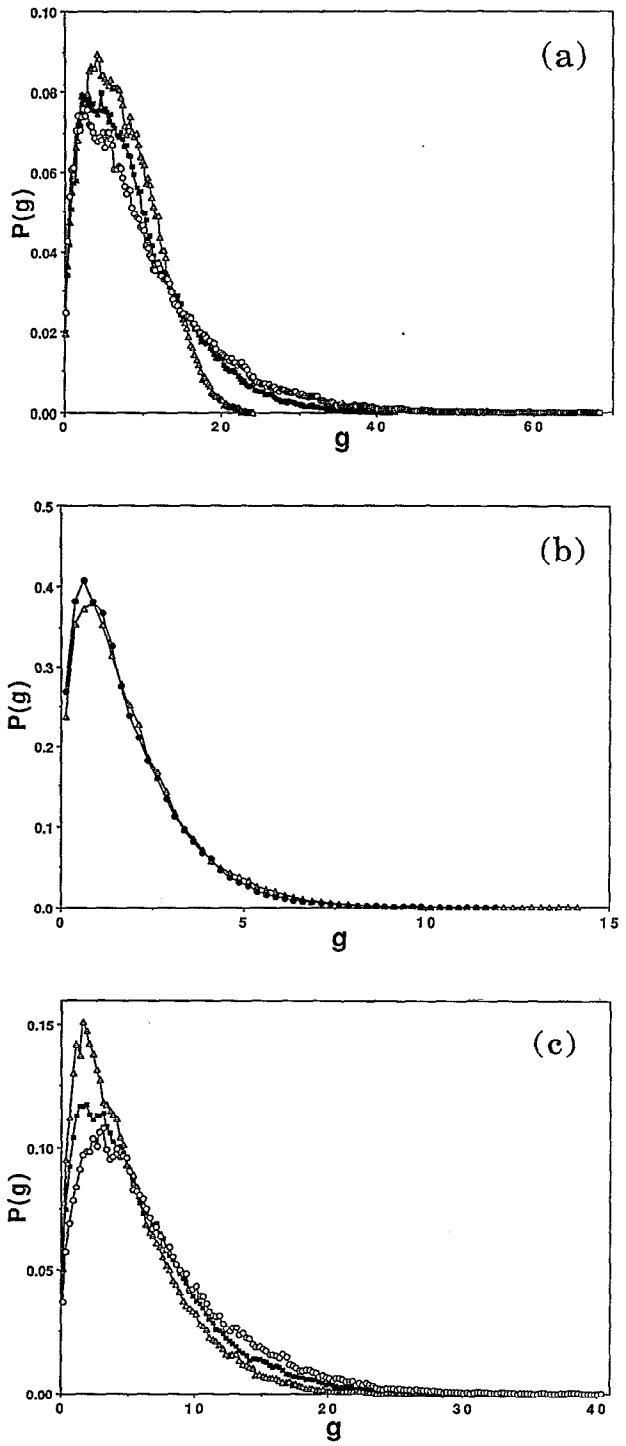

FIG. 2. The probability distribution function $P(g)$. (a) The open triangles, solid squares, and open circles are results for samples of 32, 108, and 864 dipolar soft spheres at $\epsilon_{RF}=\infty$ in PBC. (b) The open triangles and dots represent data from calculations with 32 and 500 particles at $\epsilon_{RF}=10$ in PBC. (c) The open triangles and solid squares, respectively, are values for $N=108$ and $N=256$ obtained at $\epsilon_{RF}=100$ with truncated octahedral samples in RF boundary conditions, while the open circles represent data from a 256 particle cubic system.

cluded in Table VI for each of the three orientational regions considered. Although some individual runs may suggest the existence of anisotropy in the total dipole moment (e.g., for $N=108$ and $\epsilon_{RF}=\infty$ there is a 14% difference between the observed incidence of **M** pointing at a face and at an edge), collectively the data in Table VI demonstrate no systematic trend, therefore no preferred direction, *no true anisotropy*. Similar results were obtained for all the cubic and truncated octahedral systems studied in PBC. The conclusion that these systems are isotropic at the dipole level might have been anticipated since it is well known from solid-state NMR, for instance, that the dipole–dipole interaction cannot distinguish between cubic and true spherical symmetry.[29] Recently Chandler and co-workers[13] have reported observing anisotropy in **M** in a single 250 particle simulation of a water-like liquid in PBC. If this anisotropy is in fact real (presumably due to higher order dipole–quadrupole, quadrupole–quadrupole, etc., interactions) one should be able to demonstrate that the effect is systematic and becomes small with increasing system size.

In view of the above remarks, we will assume in the remainder of this paper that $P(\mathbf{M})$ is isotropic, and hence it will be sufficient to consider the probability distribution function $P(M)$. Since M is an extensive property, $P(M)$ is not convenient for comparing results from systems of different size. Rather, we focus on the probability distribution $P(g)$, where g is the instantaneous Kirkwood correlation factor defined in Eq. (2), since g is an intensive property and its average value is directly related to ϵ through Eq. (1).

Figure 2 shows typical results for $P(g)$ for various samples of our dipolar fluid. These functions all appear qualitatively similar in form, independent of the boundary condition applied or the value of ϵ_{RF}, although some number dependence is evident. In Fig. 2(c) sensitivity to the RF cutoff is manifest as a difference between the truncated octahedral and cubic results. If we now transform our data to the form $\ln[P(g)/\sqrt{g}]$ and plot these values against g, as in Figs. 3 and 4 for $\epsilon_{RF}=\infty$, 100, and 10, we find linear behavior for larger N or smaller ϵ_{RF}. The considerable noise that appears in the tails of the distributions is due to very poor sampling at large g. However, for smaller samples, particularly for larger ϵ_{RF}, we observe in Figs. 3 and 4 that the functions deviate from ideal (i.e., that expected for an infinite system) behavior, exhibiting what we identify as finite system size effects. In PBC (Fig. 3) this effect can be simply described as a downward curvature in the data at larger values of g, whereas in RF boundary conditions (Fig. 4) there is a more apparent shift in the slope of the whole function. Furthermore, Fig. 4(b) indicates that in RF boundary conditions the deviation from the ideal result can be positive or negative, with the RF cutoff appearing to be the determining factor. Inspection of the PBC data in Figs. 2 and 3 reveals that when $P(g)$ is suppressed at large g for small N, the displaced probability is shifted to intermediate values of g. We would then expect to find a smaller value of $\langle g\rangle$ (and hence ϵ) for these systems (i.e., with $\epsilon_{RF}\geqslant\epsilon$), which is in fact what is observed in Tables II and III. We recall[14] that for any finite system g will have an upper bound, $g_{max}=N$. Clearly, for small N and large ϵ_{RF} this bound on the fluctuations in M has a direct (and consistent) impact on the distribution of values [here represented by $P(g)$] obtained in PBC. The behavior in RF boundary conditions is more complex and does not lend

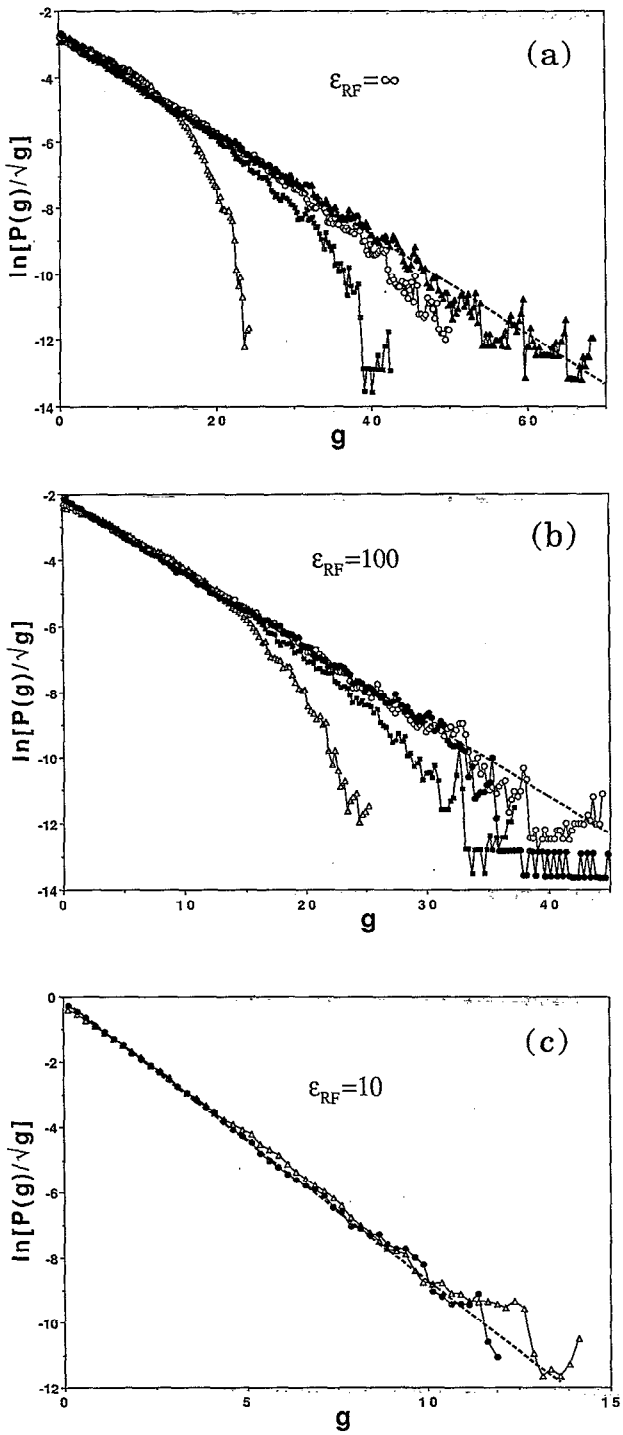

FIG. 3. The logarithm of $P(g)/\sqrt{g}$ for a dipolar fluid in periodic boundary conditions. The open triangles, solid squares, open circles, dots, and solid triangles, respectively, are data obtained for systems of 32, 108, 256, 500, and 864 dipolar soft spheres. (a) $\epsilon_{RF}=\infty$. (b) $\epsilon_{RF}=100$. (c) $\epsilon_{RF}=10$. Not all results are shown in each case. The heavy dashed line represents the ideal infinite system result.

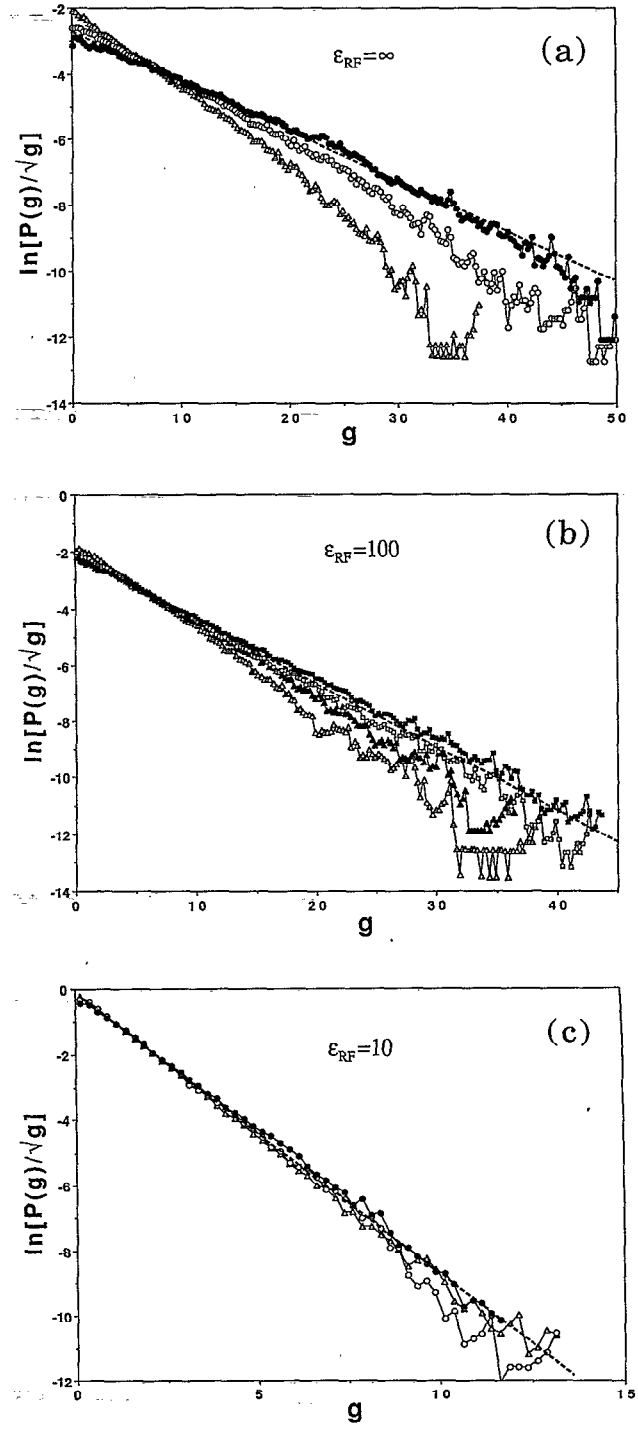

FIG. 4. The logarithm of $P(g)/\sqrt{g}$ for a dipolar fluid in RF boundary conditions. The open symbols are data obtained from systems with truncated octahedral geometry, while the solid symbols are cubic results. The triangles, circles, and squares represent $N=108$, 256, and 500, respectively. (a) $\epsilon_{RF}=\infty$. (b) $\epsilon_{RF}=100$. (c) $\epsilon_{RF}=10$. Not all results are shown in each case. The heavy dashed line represents the ideal infinite system result.

itself to a similar simple analysis. For $\epsilon_{RF}<\epsilon$ [Figs. 3(c) and 4(c)], where the fluctuations in M become relatively small, the effects of boundary conditions and system size are more subtle.

We have argued elsewhere[20] (using a figure similar to those in Figs. 3 and 4) that for sufficiently large samples, independent of cell geometry or the value of ϵ_{RF}:

$$P(g)=A\sqrt{g}e^{-\kappa g}, \tag{7a}$$

where

$$A=\frac{2\kappa^{3/2}}{\sqrt{\pi}} \tag{7b}$$

and the parameter κ (given by the slopes of the lines in Figs. 3 and 4) is trivially related to the average value of g by

$$\langle g\rangle=\frac{3}{2\kappa}. \tag{7c}$$

Not surprisingly then, we find that the value of κ, and hence the width of $P(g)$, is sensitive to changes in ϵ_{RF} (note the horizontal scales of Figs. 2, 3, and 4). It is clear from Figs. 3 and 4 that at least for large systems $P(g)$ has a simple dependence upon ϵ_{RF} through the parameter κ. In Ref. 20 this dependence was formally characterized in PBC by considering the ratio $R(\epsilon'',\epsilon')$ of two distributions at two values of the boundary condition, ϵ' and ϵ''. By taking into account the energy change of a system in PBC going from ϵ' to ϵ'', and inserting that result into the Boltzmann factor, it was shown[20] that independent of sample size (hence independent of finite size effects)

$$\ln R(\epsilon'',\epsilon')=\ln\frac{P(g,\epsilon'')}{P(g,\epsilon')}$$
$$=\frac{-2\pi\rho\mu^2}{kT}\left(\frac{1}{2\epsilon''+1}-\frac{1}{2\epsilon'+1}\right)g+B, \tag{8}$$

where B is a constant depending upon $A(\epsilon')$ and $A(\epsilon'')$.

In RF boundary conditions we begin in a similar manner, considering the dipole–dipole contribution to the total energy of the system,

$$U_{DD}(\epsilon_{RF})=U_{DD}(\epsilon_{RF}=1)-\sum_{\substack{i,j\\ r_{ij}<R_c}}\frac{(\epsilon_{RF}-1)}{(2\epsilon_{RF}+1}\frac{\boldsymbol{\mu}_i\cdot\boldsymbol{\mu}_j}{R_c^3}, \tag{9}$$

which we rewrite as

$$U_{DD}(\epsilon_{RF})=U_{DD}(\epsilon_{RF}=1)-\frac{(\epsilon_{RF}-1)}{(2\epsilon_{RF}+1)}\frac{1}{R_c^3}\sum_i \boldsymbol{\mu}_i\cdot\mathbf{M}(\Omega_i), \tag{10}$$

where $\mathbf{M}(\Omega_i)$ is defined as in the Appendix. Now for a sufficiently large system of volume V with homogeneous polarization $\mathbf{P}=\mathbf{M}/V$, one expects that any large subsample of this system of volume Ω will have polarization $\mathbf{P}(\Omega)=\mathbf{M}(\Omega)/\Omega=\mathbf{P}$, and therefore

$$\mathbf{M}(\Omega)=\frac{\Omega}{V}\mathbf{M}. \tag{11}$$

Substituting Eq. (11) into Eq. (10) and simplifying, recalling that $\Omega=4\pi R_c^3/3$, yields[30]

$$U_{DD}(\epsilon_{RF})=U_{DD}(\epsilon_{RF}=1)-\frac{(\epsilon_{RF}-1)}{(2\epsilon_{RF}+1)}\frac{4\pi}{3}M^2. \tag{12}$$

Then following the same procedure as in Ref. 20, we again obtain Eq. (8). It is perhaps worth noting that Eq. (11) is a sufficient condition for the equivalence of Eqs. (1) and (3).

In Fig. 5 we have plotted the logarithms of the ratios $R(\epsilon'',\epsilon')$ for three different pairs of ϵ'' and ϵ' for $N=108$ in RF and PBC. To within uncertainty the results in both cases

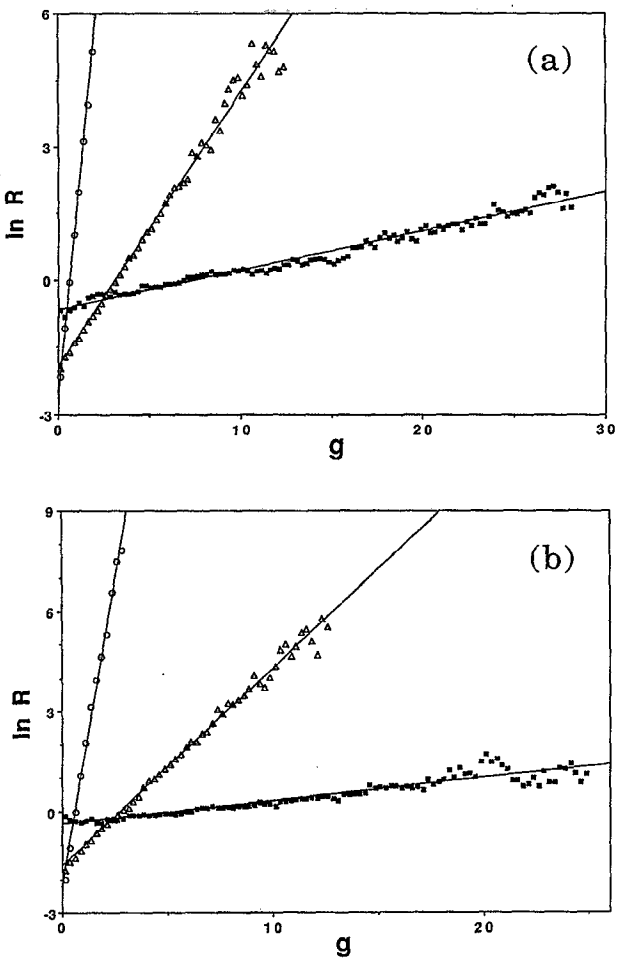

FIG. 5. $\ln R(\epsilon'',\epsilon')$ from simulations of 108 dipolar soft spheres. The solid squares, open triangles, and open circles are results for the (ϵ'',ϵ') pairs $(\infty,100)$, $(100,10)$, and $(10,1)$. The lines represent least-square linear fits. (a) PBC. (b) RF boundary conditions and truncated octahedral geometry.

appear linear in g, independent of how well Eq. (7a) is obeyed by the original distributions. The slopes determined from Fig. 5, along with data from three additional pairings with $\epsilon'=1$, are compared in Table VII with ideal values given by Eq. (8). In general the agreement is good, although better for PBC [for which Eq. (8) should be exact[20]]. This behavior is clearly related to that observed for ϵ in Tables II–V and in Fig. 1. Similar conclusions were drawn when the

TABLE VII. Values for the slope from plots of $\ln R(\epsilon'',\epsilon')$ vs g for systems of 108 dipolar soft spheres at $\rho^*=0.8$, $T^*=1.35$, and $\mu^*=2.0$.

(ϵ'',ϵ')	PBC	RF (Trunc. oct.)	Ideal[a]
(10,1)	4.13	3.65	4.26
(100,1)	4.77	4.29	4.89
(∞,1)	4.99	4.29	4.96
(100,10)	0.613	0.595	0.635
(∞,10)	0.691	0.654	0.709
(∞,100)	0.088	0.068	0.074

[a]From Eq. (8).

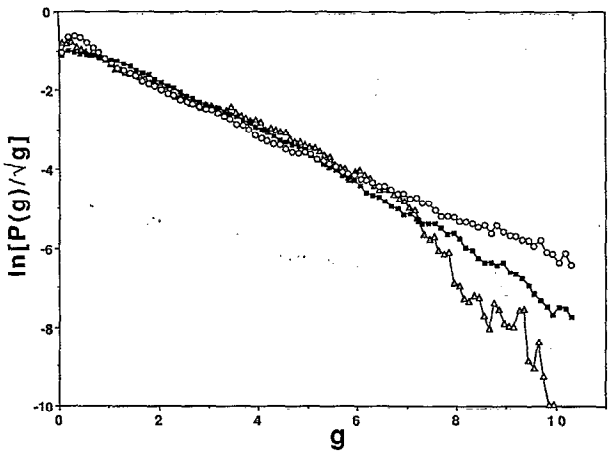

FIG. 6. $\ln[P(g)/\sqrt{g}]$ for water and for methanol at 25 °C. The solid squares and open circles represent results for 108 and 256 particle water systems, respectively, while the triangles are data from a 108 particle methanol simulation.

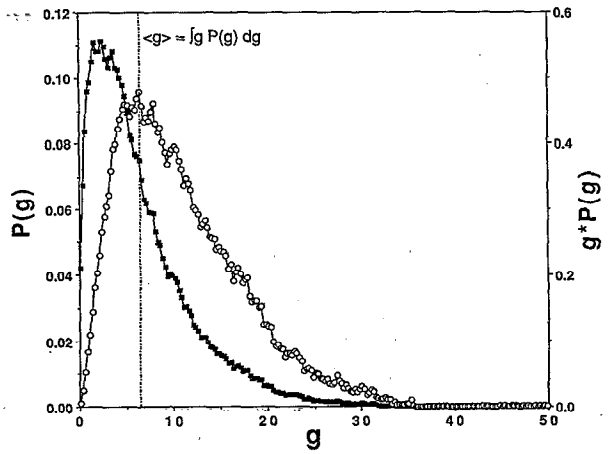

FIG. 7. Comparison of $P(g)$ and $g^*P(g)$. The solid squares represent $P(g)$ while the circles are data for $g^*P(g)$ for 256 dipolar soft spheres at $\epsilon_{RF}=100$. The vertical line indicates $\langle g \rangle$.

same analysis was applied to data from the other systems studied.

In Ref. 20, κ is expressed as the sum of two terms,

$$\kappa=\gamma+\delta, \tag{13a}$$

where

$$\delta(\epsilon_{RF})=\frac{2\pi\rho\mu^2}{kT}\left(\frac{1}{2\epsilon_{RF}+1}-\frac{1}{2\epsilon+1}\right) \tag{13b}$$

contains all ϵ_{RF} dependence [following from Eq. (8)], and

$$\gamma=\frac{2\pi\rho\mu^2}{kT}\frac{3\epsilon}{(2\epsilon+1)(\epsilon+1)} \tag{13c}$$

is the value of κ for a true infinite system (and thus independent of boundary condition). Taken together, Eqs. (7) and (13) can be viewed as yet another proof of the applicability of Eq. (1) to sufficiently large samples of polar liquids in *RF* and PBC. Moreover, in PBC (and to a lesser extent in RF) the actual shape of the distribution $P(g)$ obtained from a computer simulation of a polar liquid [i.e., its adherence to Eq. (7)] is a direct indicator of when a system is "large enough" to exhibit behavior consistent with that of a true macroscopic dielectric.

We have emphasized in Ref. 20 that our formal results for the functional form of $P(g)$ [here given by Eqs. (7) and (13)] should be *universally* applicable to any "large" spherical sample of a polar liquid. To provide further support we have accumulated data for $P(g)$ in simulations of both liquid water and liquid methanol at 25 °C. The results obtained for $P(g)$ from these calculations in PBC, shown in Fig. 6, strongly support our claim. Moreover, both the 108 particle systems in Fig. 6 exhibit finite size effects, and consequently we would expect dielectric constants determined from these calculations to be subject to systematic errors. Even though it is a less polar liquid, methanol appears more sensitive to sample size. A possible explanation for this behavior is that it will be more difficult to achieve high degrees of dipolar alignment in methanol than in water.

We now turn our focus of attention to how knowledge of the functional form for $P(g)$ can be exploited to improve or to accelerate the statistical determination of $\langle g \rangle$ in a computer simulation. In Fig. 7 we have shown the functions $P(g)$ and $g^*P(g)$. We see that the distribution function $P(g)$ has a long tail of relatively low probability which will be poorly sampled in a standard simulation. Yet, it is obvious from $g^*P(g)$ that this tail can make a significant contribution to $\langle g \rangle$. Thus, our ability to determine $\langle g \rangle$ (and hence ϵ) in a computer simulation could be improved significantly using bias sampling. The selection of configurations according to the distribution $g^*P(g)$ could be easily accomplished with a Monte Carlo algorithm.[21]

A second approach with which to improve computational efficiency would be to select specific windows (or sections) of the distribution (not necessarily adjacent) over which to sample. Knowing the functional form for $P(g)$, the complete distribution (fully characterized by the value of κ) could be easily constructed even when it has only been partially sampled. The recent investigation of Chandler and co-workers,[13] in which $P(M)$ for SPC water was assembled from a set of windows spanning the entire function, could have been simplified had they been able to assume an explicit functional form. In the present MD study we have accumulated data in four separate windows, each spanning a range of 7.5 in g for a system of 256 dipolar soft spheres in PBC at $\epsilon_{RF}=\infty$, using the trajectory mapping technique detailed above. Figure 8(a) shows the initial data from these four windows, each representing runs of only 25 000 time steps. Linear fits to the results from the individual windows give values for κ ranging from 0.122 to 0.162. However, if we fit the data from all four windows simultaneously, as shown in Fig. 8(b), we obtain $\kappa=0.1480$ which immediately yields the estimate $\epsilon=101.6$. In performing the fit in Fig. 8(b) we have taken advantage of normalization requirements

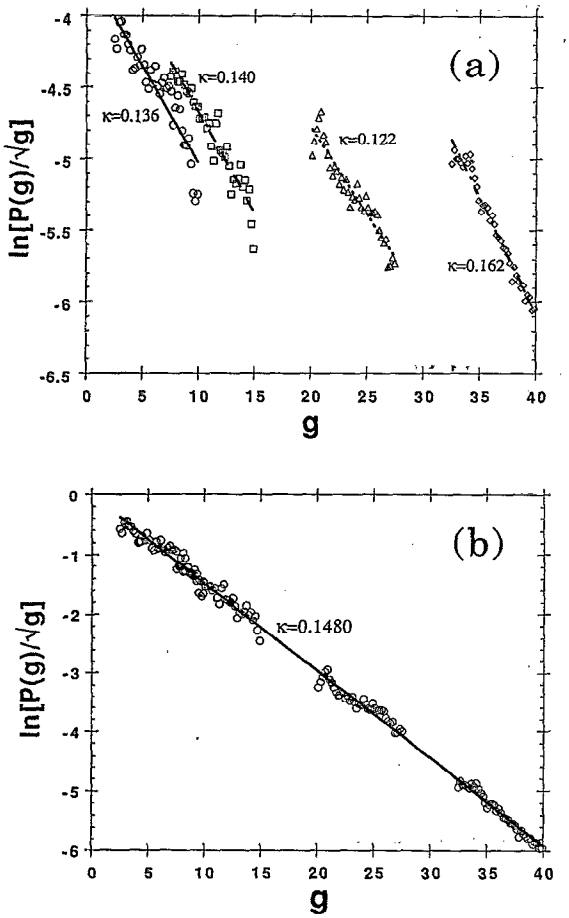

FIG. 8. Results for $\ln[P(g)/\sqrt{g}]$ from windowing MD calculations. (a) Initial raw data for the four individual windows together with their linear fits. (b) Simultaneous fit to the results from all four calculations, as discussed in the text.

and hence the relative shift of the points from each window is uniquely determined by an initial guess for the slope κ. The value for κ was then iterated to self-consistency. We point out that this procedure also gives a near optimum fit (as measured by the correlation coefficient). If we were to require only the best possible fit, we obtain a slope of 0.1534 (which still satisfies self-consistency to within 0.1%) corresponding to a dielectric constant of 98.1. We would claim that the 3.5% difference in the results from these two particular methods of fitting the data is representative of the uncertainty in the present technique (the error in the slope determined directly from the numerical fits being only 0.2%). The value of ϵ determined from Fig. 8(b) is in excellent agreement with data in Tables II and III in which Eq. (1) was employed directly. Moreover, its associated error bar, estimated at only a few percent, is comparable to those in Tables II and III even though a total of only 100 000 time steps were performed to generate all the data employed in Fig. 8. Comparing this with the 500 000 time steps carried out for each run in Tables II and III we have realized an apparent fivefold *improvement* in computational efficiency. Furthermore, our experience suggests that with a more carefully tuned windowing approach even greater improvements should be achievable.

We conclude this discussion by noting that we have also performed a limited number of Monte Carlo (MC) calculations with our dipolar system in an attempt to exploit that method to sample $P(g)$ within specific windows. Unfortunately we found that, unlike in our MD simulations, the magnitude of the total moment tended to remain very localized in these MC calculations and therefore even for windows of width 5 the overall sampling of g appeared rather poor (i.e., MC runs of about 50 000 moves per particle could not provide estimates for κ comparable to those of our 25 000 time step MD calculations). We suspect that employing several narrow windows together or exploiting collective moves of particles (instead of only single particle moves) would greatly improve the efficiency of the MC technique in calculations of this type for the dielectric constant.

IV. CONCLUSIONS

In this paper we have examined the fluctuations of the total dipole moment in polar fluids. For this purpose MD simulations have been performed for a dipolar soft-sphere fluid in both RF and PBC at $\rho^*=0.8$, $T^*=1.35$, and $\mu^*=2.0$ and detailed results have been reported for both cubic and truncated octahedral geometries. For PBC the values obtained for thermodynamic properties and the dielectric constant were found to be in excellent agreement with previous work[14] and were observed to be insensitive to the choice of simulation cell geometry. However, in RF boundary conditions the properties of interest, particularly the static dielectric constant, are more sensitive to sample size and also exhibit a dependence upon cut-off distance (which can be easily mistaken for a dependence on geometry). These observations, together with the fact that the formal analysis of the behavior of the fluctuations in **M** is more straightforward in PBC, leads us to conclude that PBC are preferable to RF in computer simulations of dipolar liquids when the dielectric properties are desired.

In the present MD study we have considered the distribution of instantaneous values for the total moment **M** and have determined the probability of **M** being in particular orientational regions as well as the average magnitude recorded for each region. From this examination we conclude that no anisotropy exists in these dipolar fluids, an observation that is consistent with formal considerations. We have also argued that if the anisotropy recently reported by Chandler and co-workers[13] for an SPC water system is real (presumably due to higher-order multipole moments), it must exhibit a clear dependence on sample size, becoming negligible for sufficiently large N.

The *universal* functional form [given by Eq. (7a)] for the probability distribution function $P(g)$, which completely characterizes the distribution of fluctuations in **M** for large N, contains only a single parameter κ, where κ can be trivially related to the average Kirkwood correlation factor $\langle g \rangle$. The numerical results for $P(g)$ reported in this study for a dipolar fluid in both RF and PBC, as well as for methanol and water systems, are entirely consistent with this functional form for large samples or small ϵ_{RF}. The formal dependence of κ

upon ϵ_{RF} given in Ref. 20 for PBC was extended in the present study to large samples in RF boundary conditions. Even for smaller systems, this formal result was found to be in good agreement with our numerical data from simulations in either boundary condition. We have clearly demonstrated that $P(g)$ is a sensitive indicator of finite size effects in computer simulations of polar liquids. Particularly for PBC, it represents an effective means of determining if the sample being employed in a simulation is large enough.

We have also considered how knowledge of the functional form for $P(g)$ could be exploited to reduce the computational requirement for the calculation of the static dielectric constant for highly polar liquids. One proposed scheme would employ biased Monte Carlo to sample according to the distribution $g^*P(g)$. A second general method would sample only small sections or windows of the full distribution and then fit the data to obtain a value for κ. A MD technique using trajectory mapping was utilized in order to calculate data for four separate windows in $P(g)$ for our dipolar system. When fit simultaneously these four sets of values gave a estimate for ϵ of precision comparable to that of results from much longer standard simulations.

Further investigation of the generalization of the current formalism for the probability distribution function $P(g)$ beyond its current limitation to linear response may provide additional insights into the effects of finite size (or saturation). The more complex behavior exhibited by our results in RF boundary conditions (such as their sensitivity to cutoff) also merit further exploration both formally and numerically.

ACKNOWLEDGMENT

We are grateful for the financial support of the Natural Sciences and Engineering Research Council of Canada.

APPENDIX: EQUIVALENCE OF EQUATIONS (1) AND (3)

Starting with the right-hand side of Eq. (3), we simply take advantage of the fact that in computing the ensemble average each spherical volume Ω_i, centered on particle $i=1$ to N, will be considered, and so we can write

$$\frac{1}{R_c^3 kT}\langle \mathbf{M}\cdot\mathbf{M}(R_c)\rangle = \frac{1}{R_c^3 kT}\left\langle \mathbf{M}\cdot\frac{1}{N}\sum_i \mathbf{M}(\Omega_i)\right\rangle = \frac{1}{R_c^3 kT}\left\langle \mathbf{M}\cdot\frac{1}{N}\sum_i\sum_{j\in\Omega_i}\boldsymbol{\mu}_j\right\rangle. \tag{A1}$$

Now in the double sum, each dipole $\boldsymbol{\mu}_j$ will be counted (included) on average

$$\tilde{n}_j = \frac{\Omega}{V}\,N = \frac{4\pi R_c^3}{3V}\,N \tag{A2}$$

times. It is also clear that in order to evaluate Eq. (A1) one does not, in principle, need to know explicitly to which volumes Ω_i $\boldsymbol{\mu}_j$ belongs, it is only required that $\boldsymbol{\mu}_j$ be included the correct number of times, n_j. Thus the sums in Eq. (A1) can be reordered and the equation rewritten as

$$\frac{1}{R_c^3 kT}\langle \mathbf{M}\cdot\mathbf{M}(R_c)\rangle = \frac{1}{R_c^3 kT}\left\langle \mathbf{M}\cdot\frac{1}{N}\sum_j n_j\boldsymbol{\mu}_j\right\rangle. \tag{A3}$$

For a dense fluid and large Ω we would expect the fluctuations in n_j to be very small (experience would suggest this is true even for systems of a few hundred particles) and so we replace n_j by its average value in Eq. (A3) to obtain

$$\frac{1}{R_c^3 kT}\langle \mathbf{M}\cdot\mathbf{M}(R_c)\rangle = \frac{1}{R_c^3 kT}\left\langle \mathbf{M}\cdot\frac{1}{N}\sum_j\left(\frac{4\pi R_c^3}{3V}\right)\boldsymbol{\mu}_j\right\rangle = \frac{4\pi}{3VkT}\langle \mathbf{M}\cdot\mathbf{M}\rangle. \tag{A4}$$

We have demonstrated numerically (see Tables IV and V) that for a dense fluid of only 108 dipolar soft spheres Eq. (A4) is already satisfied to within about 1%.

[1] J. P. Hansen and I. R. McDonald, *Theory of Simple Liquids*, 2nd ed. (Academic, New York, 1986).
[2] S. W. de Leeuw, J. W. Perram, and E. R. Smith, Annu. Rev. Phys. Chem. **37**, 245 (1986).
[3] G. N. Patey, D. Levesque, and J. J. Weis, Mol. Phys. **45**, 733 (1982).
[4] M. Neumann and O. Steinhauser, Mol. Phys. **39**, 437 (1980); Chem. Phys. Lett. **95**, 417 (1983).
[5] M. Neumann, Mol. Phys. **57**, 97 (1986).
[6] M. Neumann, Mol. Phys. **50**, 841 (1983).
[7] B. J. Alder and E. L. Pollock, Annu. Rev. Phys. Chem. **32**, 311 (1981); E. L. Pollock and B. J. Alder, Physica A **102**, 1 (1980).
[8] M. Neumann, O. Steinhauser, and G. S. Pawley, Mol. Phys. **52**, 97 (1984); M. Neumann, J. Chem. Phys. **82**, 5663 (1985); **85**, 1567 (1986).
[9] D. J. Adams and E. M. Adams, Mol. Phys. **42**, 907 (1981).
[10] D. Levesque and J. J. Weis, Physica A **125**, 270 (1984).
[11] H. E. Alper and R. M. Levy, J. Chem. Phys. **91**, 1242 (1989).
[12] K. Watanabe and M. Klein, Chem. Phys. **131**, 157 (1989).
[13] Z. Kurtovic, M. Marchi, and D. Chandler, Mol. Phys. **78**, 1155 (1993).
[14] P. G. Kusalik, J. Chem. Phys. **93**, 3520 (1990).
[15] P. G. Kusalik, Mol. Phys. **73**, 1349 (1991).
[16] P. G. Kusalik, Mol. Phys. **81**, 199 (1994).
[17] P. G. Kusalik, Mol. Phys. **76**, 337 (1992).
[18] H. G. Petersen, S. W. de Leeuw, and J. W. Perram, Mol. Phys. **66**, 637 (1989).
[19] P. G. Kusalik (unpublished results).
[20] P. G. Kusalik, Mol. Phys. **80**, 225 (1993).
[21] M. P. Allen and D. J. Tildesley, *Computer Simulation of Liquids* (Clarendon, Oxford, 1989).
[22] D. J. Adams, Inf. Q. MD MC Simulations **10** (1983).
[23] D. J. Evans and G. P. Morriss, *Statistical Mechanics of Nonequilibrium Liquids* (Academic, San Diego, 1990).
[24] G. P. Morriss and D. J. Evans, Phys. Rev. A **39**, 6335 (1989).
[25] H. J. C. Berendsen, J. R. Grigera, and T. P. Straatsma, J. Phys. Chem. **91**, 6269 (1987).
[26] M. Haughney, M. Ferraria, and I. R. McDonald, J. Phys. Chem. **91**, 4934 (1987).
[27] I. M. Svishchev and P. G. Kusalik, J. Phys. Chem. **98**, 728 (1994); J. Chem. Phys. **99**, 3049 (1993).
[28] I. M. Svishchev and P. G. Kusalik, J. Chem. Phys. **100**, 5165 (1994).
[29] M. Hehring, *High Resolution NMR Spectroscopy of Solids* (Springer, Berlin, 1976).
[30] It is also possible to obtain this result by first ignoring variations in $\mathbf{M}(\Omega_i)$ and replacing it by its average value $1/N\Sigma_i\mathbf{M}(\Omega_i)$ and then employing assumptions identical to those used in the Appendix.